Available online at www.garmian.edu.krd

Passer Journal of Basic and Applied Sciences

Passer 7 (Issue 1) (2025) 686-697

Original Article

The Anti-bacterial Efficacy of Palladium Nanoparticles Synthesized from Red Onion Extract

Nazar Khalaf Mahan * [1], Aliyaa Abdullh Urabe [1], Shaimaa Ahmed Kadhim [2]

[1] *Department of Physics, College of Science, Mustansiriyah University, Baghdad 10001, Iraq.*
[2] *College of Education for Pure Science/Ibn Al- Haitham, University of Baghdad, Baghdad 10001, Iraq*

Received 23 January 2026; revised 03 May 2026;
accepted 15 May 2026; available online 01 July 2026

DOI: 10.24271/PSR.2026.572109.2553

ABSTRACT

This study utilized the pulsed laser ablation in liquid (PLAL) technique to produce palladium nanostructures in a plant extract as the medium. Palladium nanoparticles Pd NPs were synthesized at laser energy levels of (760, 860, and 960 mJ), (150 pulses) at a wavelength of λ = 532 nm. The analysis of the morphological structural, optical, and chemical properties of all samples as been conducted. From XRD, it found the Pd nanoparticles, indicating crystal sizes of (28.6, 16.4, and 9.2) nm, respectively. By FE-SEM of Pd was used to study the morphologies of the sample, where decrease in the particles diameters with increase in concentration. Using (TEM) and particle size histograms elucidated morphological variations and particle distribution. Atomic force microscopy (AFM) of Pd were found to have average grain size of (12.2, 19.1, 23.8) nm, respectively. Pd NPs was discovered to have a band gap of (4.4, 4.2, 4.1)eV. Pd NPs samples were used to evaluate anti-bacterial efficacy was assessed against Staphyloccusn aureus (Gram-positive) and *Eschericia coli* (Gram-negative) a utilizing the agar well diffusion method. Pd NPs produced at 960 mJ demonstrated enhanced Anti-bacterial efficacy, especially against *E. coli*, because to their increased concentration and reduced particle size.

Keywords: Palladium nanoparticles (Pd NPs), laser ablation, E. coli, and FE-SEM.

1 Introduction

Materials with exceptional properties at the nanoscale, from (1-100) nanometers, have contributed to the creation and development of physical, chemical, life sciences, and engineering [1,2]. This technology possesses the superior capabilities and distinctive characteristics of nanomaterials, such as high surface area, precise dimensions, and specific electrical and structural charges, compared to aggregate materials. This makes it suitable for various biological and medical applications [3,4], catalytic [5], and optical [6]. Recently, the misuse of antibiotics has led to serious problems and the emergence of drug-resistant strains of bacteria, posing a significant threat to human health. This necessitates the development of new materials with unique properties to help overcome these challenges, leading to the creation of nanoparticles to deliver treatments to targeted cells [7]. Nanoparticles extracted from various plants provide an exciting and important pathway in the development of biological and chemical applications. Their environmentally friendly production, biocompatibility, and potential for medical uses make them a subject of research in therapeutic care fields. This highlights the less toxic elements, including precious metals such as silver, gold, palladium, and zinc. However, silver nanoparticles are highly toxic due to gradual oxidation and the release of highly reactive silver ions Ag^{+} [8,9]. Nano palladium, because of its significant advantages in the fields of biomedicine, life sciences, and pharmacy, which are the result of an increased surface-to-volume ratio, they have been used inhomogeneous and heterogeneous catalaysis, and duo to their great important, palladium nanoparticles were develop [10-12]. The environmentally friendly production of metal nanoparticles by the utilization of plant extracts offers an alternative that is both sustainable and economical. Under this methodology, the presence of polyol compounds in the extracts helps to reduce the amount of metal ions, while the presence of water-soluble heterocyclic compounds contributes to the stabilization of nanoparticles [13-15]. Because antibiotic resistance arises when microorganisms that cause disease develop the ability to withstand exposure to treatments designed to remove them, it has become one of the most important concerns that the worldwide public health community is currently confronting. *Staphyloccusn aureus* (*S. aureus*) and *Eschericia coli* (*E. coli*) are examples of bacterial species that have been the subject of extensive research. Typically, the lower intestines of warm-blooded species are home to the gram-negative bacterium known as *E. coli*. This bacterium

* Corresponding author
E-mail address aliyaa.a@yahoo.com (Instructor).
Peer-reviewed under the responsibility of the University of Garmian.

is able to flourish in both the presence and absence of Oxygen, with the ideal temperature being 37 degrees Celsius. There are specific strains of *E. coli* that are capable of causing significant foodborne diseases, despite the fact that the majority of *E. coli* strains are innocuous and are a component of the regular gut flora. *S. aureus*, on the other hand, is a Gram-positive bacterium that is frequently found on human skin and in nasal passages. It is capable of producing a broad variety of infections, ranging from skin disorders that are superficial to diseases that affect the entire body [16-18]. In this study, report the synthesis of Pd nanoparticles by ablation in red onion extract usin a Nd:YAG, We investigate Pd NPs structural, optical, and antibacterial effect. Pd NPs has been used in various applications, including antibacterial activity, yet it did not achieve a satisfactory inhibition rate. However, we review of previous studies has not found any publication that discuss the interaction of palladium nanoparticles with plant extract, especially the when it comes to using (red onion extract) to antibacterial bacteria active, which is a direct and effective method. The antibacterial *Staphyloccusn aureus* and *Eschericia coli* were used to evaluate the efficacy of these Pd NPs. The result of this study is that it controls the size of the nanomaterial and the inhibition rate. Therefore, we indicate that this is the first report of a Pd NPs with rid onion extract.

2 Methods and Materials

2. 1 A-synthesis of red onion aqueous extract

Fresh onions were washed (20 gm) and sliced before being cooked in 500 milliliters of deionizer water for 10 minutes. Following the chilling process, the Mixture was filtered using conventional filter paper in order to get a transparent extract. This extract was utilized as the medium for the synthesis of palladium nanoparticles (Pd NP).

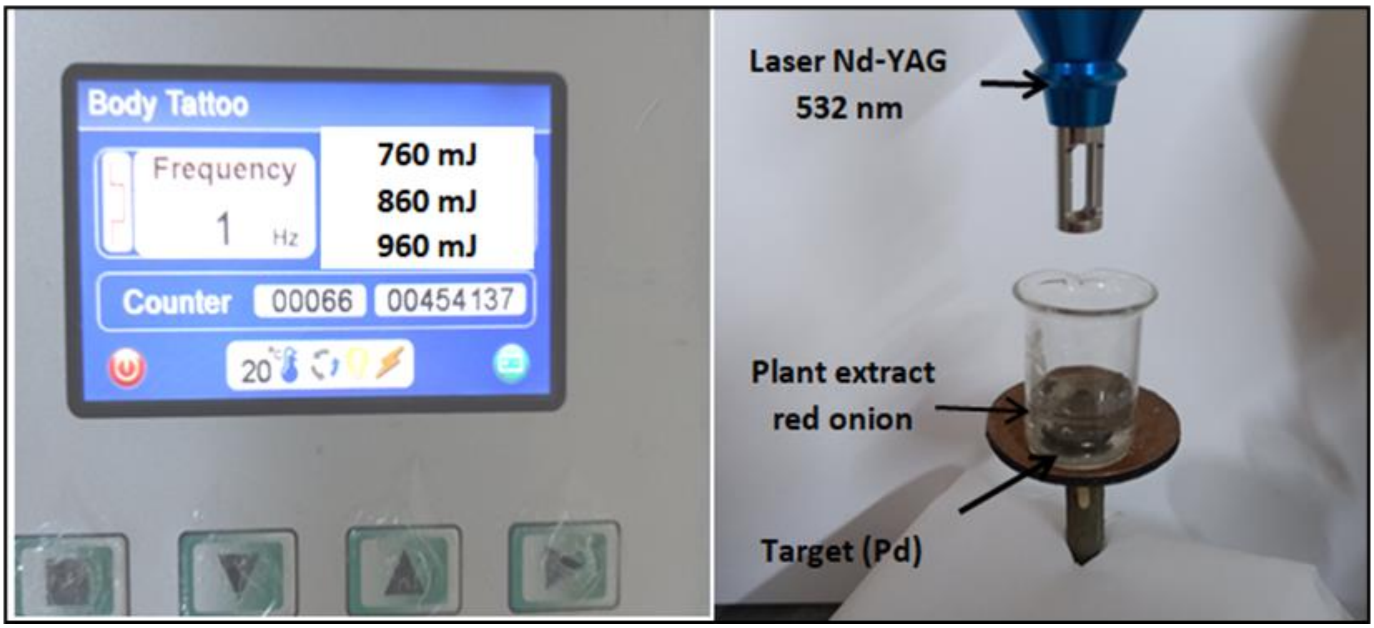

Figure 1: Image from the laboratory for preparation Pd NPs by PLAL different energy.

2. 2 Green synthesis of nanoparticles

A Nano palladium was prepared from a target (Pd, 1 cm diameter, thickness 3 mm, 99.91% purity) with 3 ml of plant extract inside a beaker placed on a rotating base to ensure even distribution of the 1 Hz laser pulse. The laser beam was focused into an 80 mm convex lens on the upper surface of the target at energies of 760, 860, 960 mJ in 150 pulses. In order to get the best possible ablation conditions, the target was positioned eight centimeters away from the laser source. Figure (1-b) depicts the utilization of a Q-switched Nd:YAG laser with a wavelength of 532 nm, respectively. Pd NPs were prepared at a concentration of 70 gm/mL for use in collecting the material for upcoming experiments.

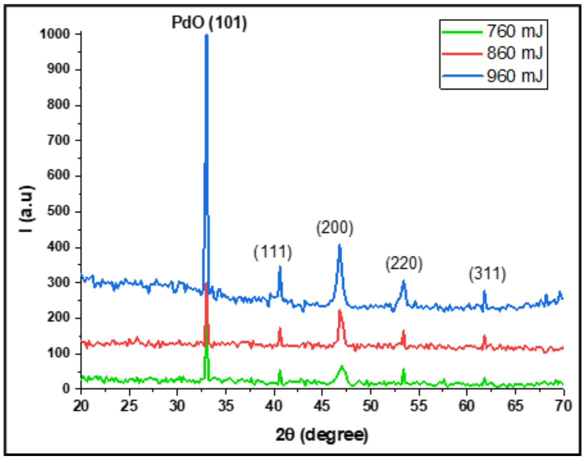

Figure 2: XRD analyses were conducted on samples synthesized under varying laser ablation energies of 760, 860, and 960 mJ.

2. 3 The Muller-Hinton (M-H)

Agar used in the subsequent investigations was prepared by dissolving 38 grams of M-H face powder in (1 liter) of distilled water, heating and stirring the mixture until it was fully dissolved, and then autoclaving it for fifteen minutes in 121° C to sterilize it. In conclusion, the medium that had been cooled to approximately 50 degrees Celsius was placed onto petri dishes, where it was allowed to solidify for approximately 15 minutes before being inverted and stored at a temperature of 4 degrees Celsius.

2. 4 Antibacterial activity

The (Pd NPs) ave Anti-bacterial activity, which were generated under different laser fluences, was studied against two different bacterial strains. These strains were Gram-positive Stapylococoous aureus and Gram-negative *Escherichia coli*. The method of dispersion in leasing is the method followed along with the unification of the methods used for that [18]. Both Gram-positive *Stapylococoous aureus* (*S. aureus*) and Gram-negative *Escherichia coli* (*E. coli*) were chosen as the organisms to be studied. After being prepared and sanitized using autoclaving at 121 degrees Celsius, 15 pounds per square inch for fifteen minutes, nutrient agar was cooled to 45–50 degrees Celsius before being placed onto Petri plates. The bacterial suspensions were adjusted to approximately 10^5 CFU/mL, and then the agar surfaces were infected with them once the solidification process was complete. In order to conduct the experiment, wells were filled with Pd NP solutions, and sterile distilled water was used as the controls. It was measured according to the size of the inhibition zones after incubating the plates at 37° C for afull day (24 hours) was measured in millimeters. In order to further evaluate the effectiveness of Anti-bacterial agents, a co-culture approach was utilized. Pd nanoparticles that were manufactured using laser energy of 760, 860, and 960 mJ were combined with nutritional broth that included the organisms that were being tested in a ratio of one to one. The preparation of control samples, which consisted solely of nutritional broth, took place simultaneously. In order to determine the level of bacterial viability, all cultures were subjected to a 24-hour incubation period at 38 degrees Celsius. Subsequently, aliquots of 1 milliliter were successively diluted from each sample, with the concentrations ranging from 10^{-1} to 10^{-8}.

For the purpose of determining the level of Anti-bacterial activity exhibited by the produced palladium nanoparticles (Pd NPs), samples that had been serially diluted were placed onto nutrient agar plates in an aseptic manner. To determine the degree of growth inhibition, bacterial colonies were counted after being incubated at 37 degrees Celsius for twenty-four hours. The formula that was developed by Ghosh et al. [19] was utilized in order to determine the percentage reduction in the growth of bacteria in the text as Equation (1).

$$X\ (\%) = \frac{(A-B)}{A}\ X\ 100 \qquad (1)$$

Where X represents the reduction rate, A is the number of colonies observed in the control average, and B is the number of colonies in the treated medium. This quantitative approach enabled a comparative evaluation of the antimicrobial efficacy of Pd NPs synthesized under different laser fluences.

3 Characterizations

This study employs pulsed laser ablation in liquid (PLAL) to synthesize palladium nanostructures using a plant extract as the stabilizing medium. By integrating green chemistry principles with advanced nanofabrication techniques, this approach aims to address the escalating issue of microbial resistance a critical challenge across multiple sectors with a particular emphasis on enhancing antimicrobial efficacy in biomedical applications.

X-ray diffraction (XRD) produces a series of diffraction peaks with distinct positions and intensities, each of which reflects the underlying crystal structure and enables phase identification [20,21].

Atomic force microscopy (AFM) is a high-resolution scanning probe technique that images surface topography at the atomic and molecular scales by detecting interactions between a sharp tip and the sample. In addition to visualization, AFM enables the measurement of nanomechanical properties such as elasticity, hardness, and adhesion under various conditions, including air, vacuum, and liquid environments [22].

Using a transmission electron microscopy, morphology characteristics of nanoparticles solution, including particle shape and size, were determined. TEM was carried out utilizing a ZEISSLEO 912 AB-100 KV TEM apparatus at Day petronic, Tehran (Iran 3.6.3 Optical properties).

Test FE-SEM was used to analyze agglomerates, surface morphology, shape and particle size of Pd NPs samples deposited on porous silicon. The samples have been examined FE-SEM "(EBSD Instrument: ZEISS SIGMA VP)" in Daypetronic Co.

Tehran-Iran. The elemental structure, proportion, and purity of each metal in the structured powder of synthesized Pd NPs/P.

The optical properties of the NPs solution were examined using UV-Vis spectroscopy “using a Shimadzu UV-1800/Japan Spectrophotometer” with a wavelength lamp with a wavelength lamp of (200-900) nm, at the applied science department, technological university, Iraq Baghdad).

The antibacterial efficacy of the synthesized samples (P,760, 860, and 960 mJ), incorporating plant extract, was assessed against both Gram-negative and Gram-positive bacterial strains using the agar well diffusion technique. This method enabled the evaluation of inhibition zones, providing comparative insights into the antimicrobial performance of each sample as a function of laser ablation energy. First, approximately 20 mL of sterile Mueller–Hinton (MH) agar was poured into sterile Petri dishes and allowed to solidify. Bacterial strains, isolated from stock cultures, were cultured in broth and standardized to a concentration equivalent to the 0.5 McFarland standard. Using a sterile cotton swab, the standardized inoculum was then evenly spread across the surface of the MH agar plate. Wells of 6 mm diameter were subsequently punched into the agar using a sterile cork borer or pipette tip.

4 Results and Discussions

Figure 2 illustrates the X-ray diffraction (XRD) patterns of the palladium-based nanostructures that were created. These patterns were measured via a 2θ range that extended from 20° to 70°. The face-centered cubic (FCC) crystal structure of palladium (FCC) (Space Group 141 / JCPDS - No. 46-1043) is confirmed by the presence of prominent diffraction peaks at approximately 33.1 degrees, 40.6 degrees, 45.8 degrees, 53.4 degrees and 61.3 degrees. These peaks correspond to the lattice planes (111), (200), (220), and (311) respectively. Furthermore, a peak that is located close to the angle of 2θ = 33° is assigned to the (101) plane, which serves as evidence for the existence of palladium oxide (PdO) phases [23]. When the laser fluencies were 760, 860, and 960 mJ, respectively, the cristillin size was calculated using Scherrer's equation were produced were roughly 28.6 nm, 16.4 nm, 9.2 nm and 8.7 nm. It was accompanied by an increase in dislocation (12.3, 37.2, 102.8, and 130) respectively and microstrain (1.12, 2.11,3.51, and 3.96) respectively, [24]. This increases surface roughness (AFM) and increases particle dispersion (TEM) [25].

It was observed that there is a distinct inverse relationship between the laser fluence and the size of the crystallites, which suggests that a higher energy input could aid the production of nanostructures that are finer [26].

Pd nanoparticles (Pd NPs) are placed on substrates, an area measuring 500 nm × 500 nm. Figure 3 displays atomic force microscope (AFM) images of the three-dimensional surface scan over this area. The preparation of these samples was accomplished through the utilization of laser ablation at different energies of 760, 860, and 960 MJ through 2nd harmonic motion. It appears from the findings that the surface became more and more abrasive, and that it was almost entirely loaded with nanoparticles. Table 1 provides a summary of the surface parameters that were acquired from AFM measurements that were performed using the Raman technique. In terms of size, shape, and height, the study performed by the AFM demonstrates that the nanoparticles are not distributed in a uniform manner. The greatest (Rmax) and minimum (Rmin) particle heights were used to establish the roughness range, and the largest pore diameter, highest average roughness, and roughness range were recorded at a laser wavelength of 532 nm. This was done in accordance with the American ISO standards [27].

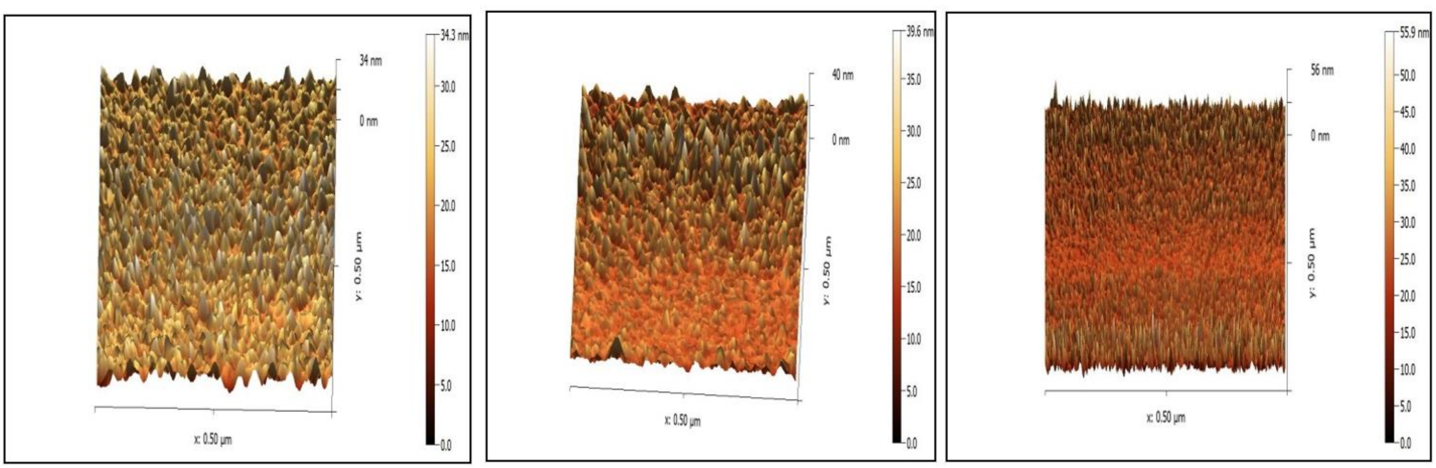

Figure 3: AFM imageis of Pd NPs at differaction laser energy 760, 860, and 960 mJ with λ= 532.

Table 1: AFM counting of Pd NPs ablated at 760, 860, 960 mJ, with λ laser energy 532 nm.

Sample (mJ)	Average RMS	Average dia.	Roughness

	(nm)	**(nm)**	**Ra (nm)**
760	2.6	12.25	1.39
860	3.8	19.14	1.86
960	5.1	23.80	3.22

Figure 4 shows TEM images of a (PdNPs) solution prepared at varying energies using the second-harmonic laser ablation method with 150 pulses. The spherical shape and average size (68.8, 27.6, and 26.6) nm respectively, the average particle sizes were measured to be around and. These values refer to the average particle size. Decrease with increasing stimulation energy [28].

The organic compounds in the plant extract act as both reducing and stabilizing agents for Pd^{2+} ions, leading to the formation of PdNPs with the desired characteristics [29].

Figure 5 illustrates the high resolution of the surface morphology of (Pd NPs), ranging in shape from rock-like aggregates to spherical ones, and some are rods with decreasing size [29].

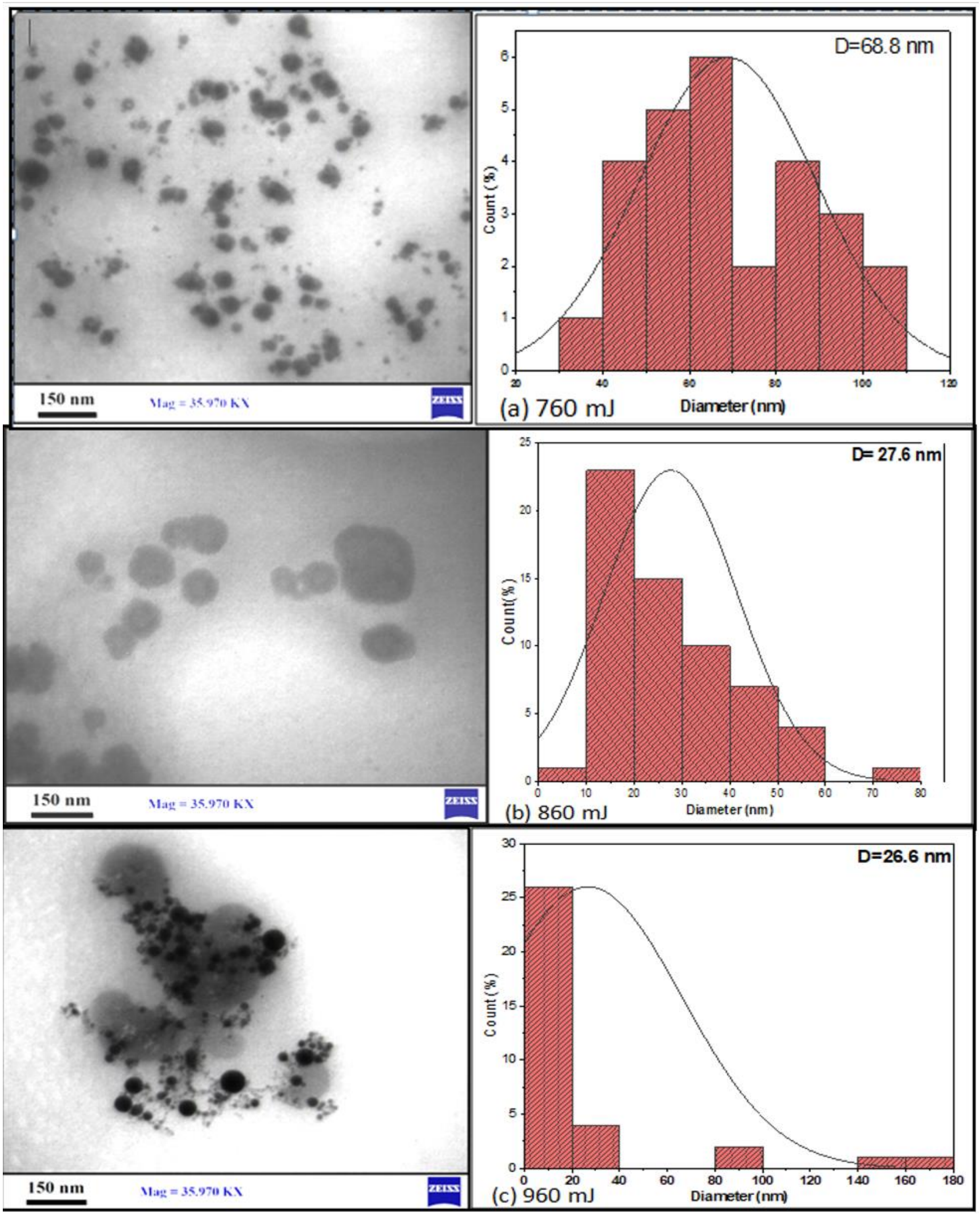

Figure 4: Image of TEM and chart distribution for Pd NPS laser ablation with energy (a)760 mJ, (b)860 mJ and (c) 960 mJ.

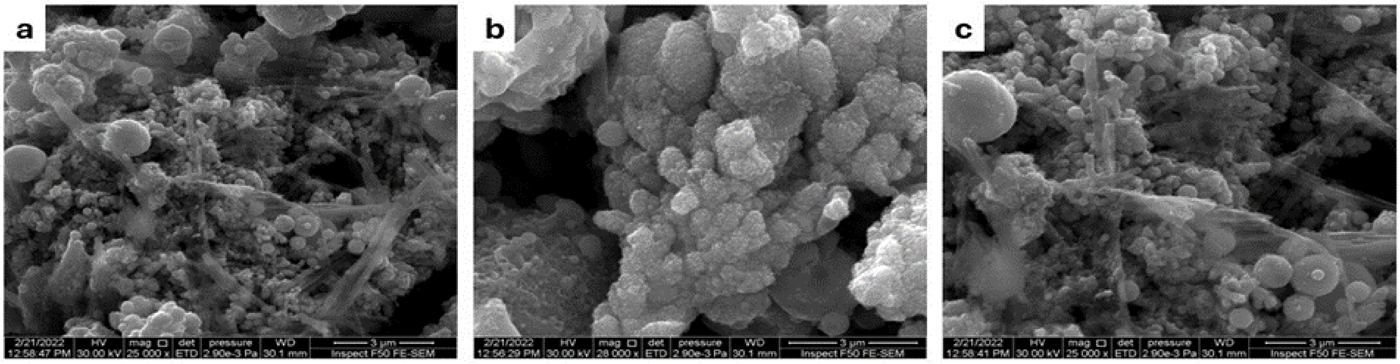

Figure 5: FE-SEM images of (Pd NPs) 760mJ, 860 mJ, and 960mJ.

As can be seen in Figure 6, the Pd nanoparticles that were manufactured at increasing laser energy displayed elevated absorption peaks at wavelengths of 390 nm, 300 nm, and 314 nm, respectively. As can be seen in Figure 7, the energy band gaps that correspond to certain energies were determined to be (5, 4.2, and 4.1)eV respectively. Crystallite size and optical band gap were shown to have an inverse correlation with laser ablation energy [30]. This correlation was found to exist between the two variables. As the laser intensity rose, it was noticed that the diameters of the particles and the band gap values gradually decreased 0throughout the experiment. This behavior is mostly related to the quantum confinement effect, which becomes more pronounced as the particle size decreases. This, in turn, causes the electrical characteristics of the nanostructured material to be altered [31].

Figure 7 shows the energy band gap in (Pd NPs) which was determined fore its UV-Vis absorption using the equation presented by wood and Tauc:

$(\alpha\, h\nu)1/\gamma = (h\nu - E_g)n$ (2)

In this study, the absorption coefficient (α) was analyzed using the Tauc relation, (h) is Plancks constant, (Eg) represents the optical band-gap energy, (ν) is the frequency of incident photon, (γ) is a parameter reflecting the nature of the band gap transition (The transfer was direct to the Pd NPs), and (n) is constant that depends on the nature of the electronic transition [32].

The Eg values were determined by extrapolating the linear portion of the Tauc plots to the point where α =0.

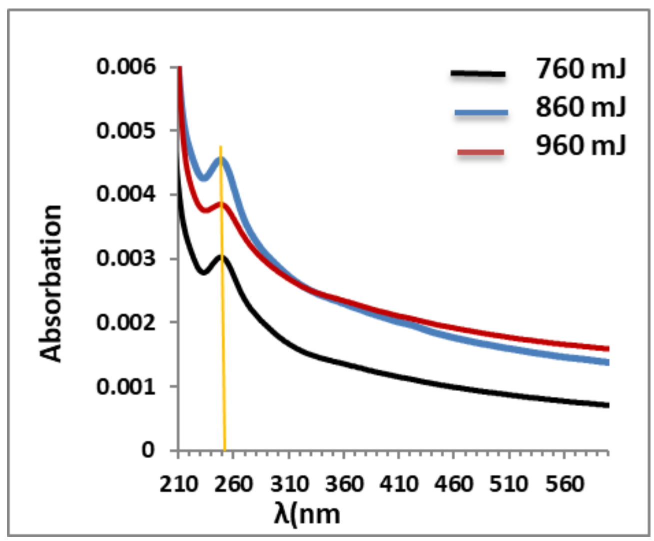

Figure 6: The optical absorbance spectra of palladium nanoparticles synthesized at laser fluences of 760, 860, and 960 mJ.

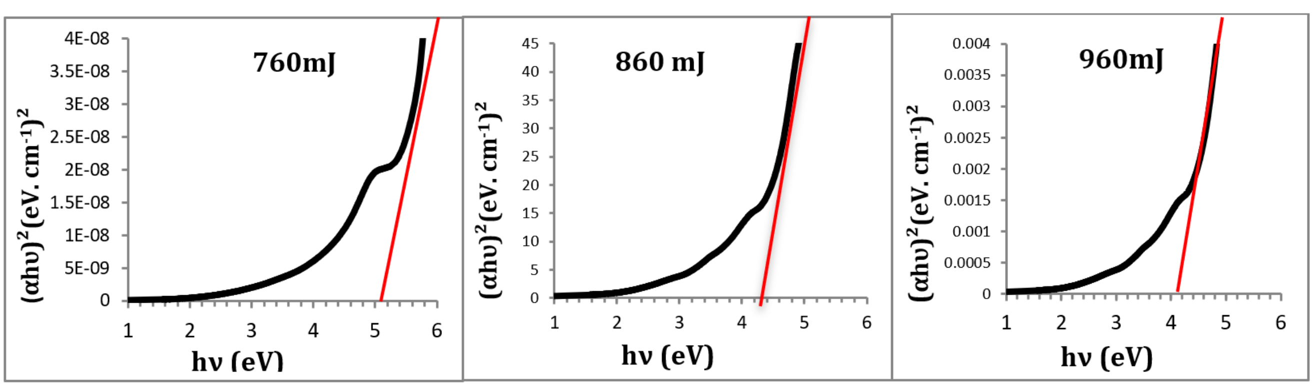

Figure 7: The variation in energy band gap values of palladium nanoparticles synthesized at laser fluences of 760, 860, and 960 mJ.

4. 1 Anti-bacterial activity

Used 70 gm/mL of the prepared samples (B,760, 860, and 960 mJ) were dispensed into these wells. The diameters of the inhibition zones were measured and recorded after incubating the cultured paltered plates at 37° C [33,34] . The effect of the plant extract increased the activation of the nanomaterial during the inhibition process, compeer [35,36]. We observe an increase in the antibacterial effectiveness of palladium nanoparticles with increasing laser intensity due to the increased density of palladium nanoparticles, especially at 960 mJ. This may be due to a decrease in crystal size, accompanied by an increase in the surface roughness of the sample (AFM) and an increase in particle agglomeration (FE-SEM). And the results of ultraviolet-visible radiation [37-39]. The presence of the plant extract in the synthesis of the palladium nanoparticles, which acts as a stabilizing and reducing agent, contributed to this [40,42]. The resulting damage in bacterial cells is due to a defect in the transport of metals and proteins to and from cell membranes, or to stress on the cell wall, which causes the production of the enzyme lactate dehydrogenises and ultimately cell damage [43, 44].

Figure 8 illustrates the activity results of the Anti-bacterial at different concentrations, and all the details are also explained in Table 2.

Table 2: Explain the Anti-bacterial activity of nanoparticles.

Anti-bacterial analysis (Zone of inhibition (mm))					
Sample	**Die-ionize water (A)**	**Redonin extract (B)**	**Pd NPs at 760 mJ (C)**	**Pd NPs at 860 mJ (D)**	**Pd NPs at 960 mJ (E)**
E. coli	6	14	17	18	26
S. aureus	6	17	20	22	30

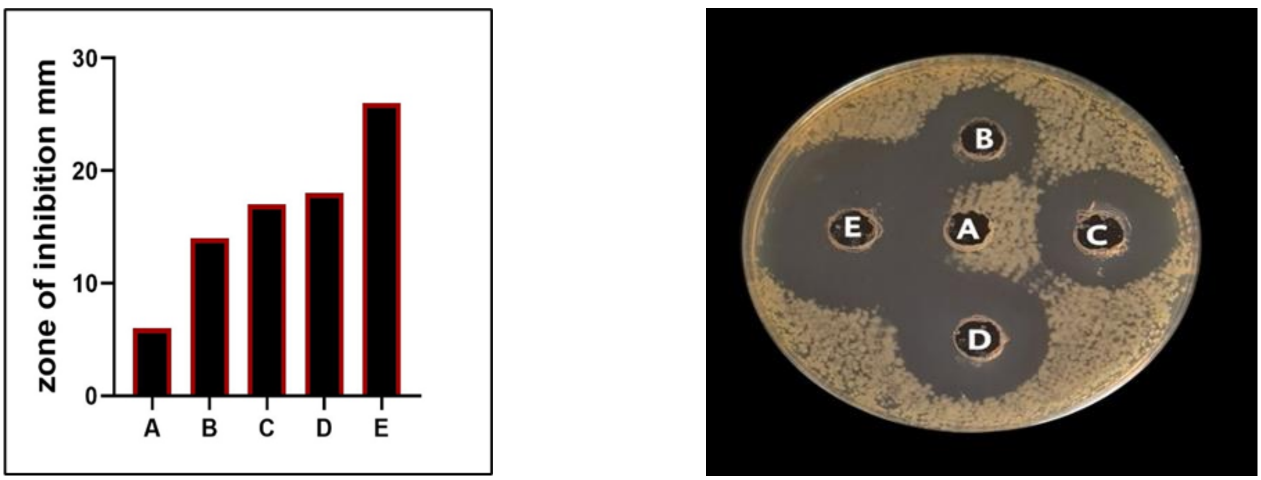

Figure 8: Antibacterial activity of (Pd NPs) against *E. coli*. (A: Control), (B:Red onion extract), (C:Pd 760mJ), (D:Pd 860 mJ), and (E:960 mJ).

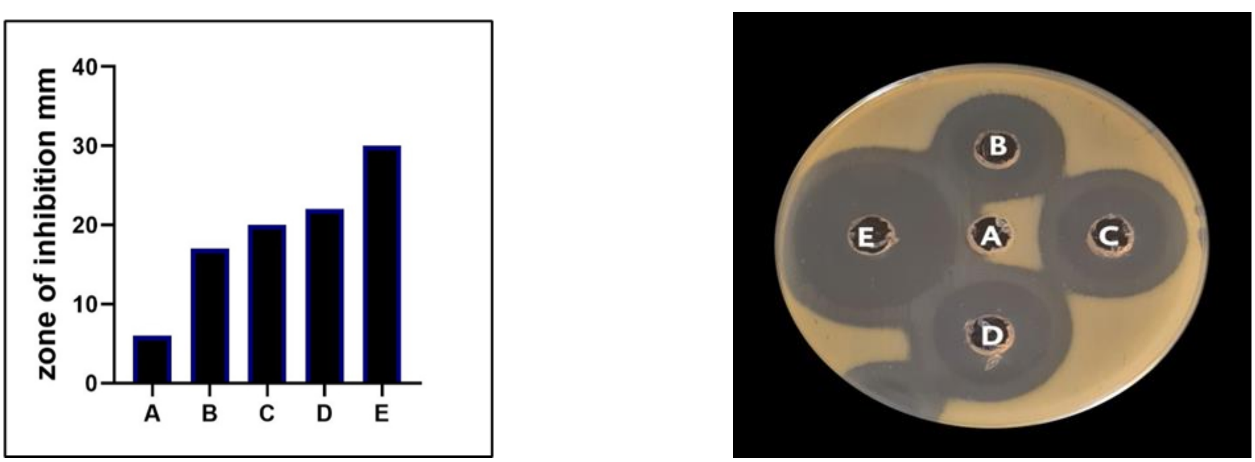

Figure 9: Antibacterial activity of (Pd NPs) against *S. aureus*. (A: Control), (B:Red onion extract), (C:Pd 760mJ), (D:Pd 860 mJ), and (E:960 mJ).

5 Conclusion

Through the use of laser ablation in plant extract at a wavelength of 532 nm and with energies ranging from 760 to 960 mJ, it was possible to successfully produce Pd nanoparticles. These palladium nanoparticles exhibited considerable inhibitory activity when they were present in the presence of plant extracts. Methods such as X-ray diffraction (XRD), transmission electron microscopy (TEM), and ultraviolet - visible spectroscopy (Uv-Vis) were utilized in order to conduct a comprehensive analysis of the structural and optical features of the Pd nanoparticles that were created. In the course of the characterization, it was discovered that an increase in the optical band gap occurred concurrently with a reduction in the size of the crystallites at the nanoscale. The sample that was generated at a laser fluence of 960 mJ had the highest inhibition rate in bacteria *E. coli* when compared to the other samples that were evaluated. As a result of the red onion extract's ability to prevent particle aggregation, homogenous, and reduce crystal size, this boost is most likely the result of the combined impacts of reduced particle size and modified electronic structure.

Authors' contributions

Author contributions **Nazar Khalaf Mahan, Aliyaa Urabe** conceived Pd NPs with different energy and supervised the study and designed the experiments. **Aliyaa Urabe** carried out the XRD, FE-SEM, TEM and the absorption measurements. **Shaimaa A. Kadhim** drafted the initial version of the manuscript, and commented on the results, provided ideas for the study, and reviewed the manuscript.

Funding

No funded

Acknowledgments

The authors would like to thank the University of Mustansiriyah, Baghdad, Iraq for the logistic supports this work.

Conflicts of Interest

The authors have no conflict of interest

References

[1] Shrivastav A, Khapekar Y, Soni D, Sankathala S, Das S. Green Synthesis of Palladium Nanoparticles Using Medicinally Important Plant Extracts. Transactions of the Indian Institute of Metals. **78**(4), 95, (2025 Apr).

[2] Aziz W, Abd Urabe A. Chemical preparation of iron oxide nanoparticles using plants extracts in antibacterial application. International Journal of Bioorganic Chemistry. **4**(1), 1 (2019).

[3] Paul S, Chowdhury AA, Basak N. Phyto-Assisted Biogenic Nanoparticles of d^8 (Nickel, Palladium, and Platinum) System): An Advancement in Medicinal Chemistry. InPlant-Associated Medicinal Nano-Chemistry, 143-163, CRC Press, (2026).

[4] Urabe AA, Aziz WJ. Assessment of antimicrobial activity of phytofabricated iron oxide nanoparticles.

[5] Urabe AA, Nayef UM, Kamel R. Studying the photocatalytic characteristics of Pd nanoparticles created by second harmonic laser ablation. Plasmonics. **18**(5),1735-41, (2023 Oct).

[6] Urabe AA, Nayef UM, Kamel R. Improved spectral responsivity of porous silicon after the deposition of palladium nanoparticles via laser ablation at different laser energies. Modern Physics Letters B. **37**(25), 2350096, (2023 Sep 10).

[7] Soussi A, Tomasoni AM, Mouak S, Hakmi M, Ibrahimi A, Sacile R. The Impact of Hazardous Chemicals on Human Health and the Environment: State of the Art and Risk Assessment Tools. Integrated Science for Sustainable Development Goal 3: Universal Good Health and Well-Being. **12**, 165-200, (2024 Dec).

[8] Seatle ND, Akinfenwa AO, Pearce KM, Sagbo IJ, Benjeddou M, Hussein AA. Green Synthesis of Au-Pd Bimetallic Nanoparticles Using Aspalathin and Their Toxicity Study. Molecules. **31**(5), 910 (2026 Mar 9).

[9] Lakkakula JR, Naik HS, Divakaran D, Srivastava R, Raut R, Uddin I. Biocompatibility and photothermal efficiency of silver palladium (AgPd NPs) and gold palladium (AuPd NP) bimetallic nanoparticles synthesized using Aloe barbadensis Linn. leaf gel. Cytotechnology. **78**(2), 55, (2026 Apr).

[10] Urabe AA, Nayef UM, Kamel R. Synthesis of Pd NPs via laser ablation in liquid assisted with magnetic field on silicon nanostructure for gas sensor. Surface Review and Letters. **30**(10), 2350067, (2023 Oct 17).

[11] Phan TT, Huynh TC, Manivasagan P, Mondal S, Oh J. An up-to-date review on biomedical applications of palladium nanoparticles. Nanomaterials. **10**(1), 66, (2019 Dec 27).

[12] Singh P, Haloi P, Singh K, Roy S, Sarkar A, B SL, Choudhary R, Mohite C, Chawla S, Konkimalla VB, Sanpui P. Palladium nanocapsules for photothermal therapy in the near-infrared II biological window. ACS Applied Materials & Interfaces. **15**(33), 39081-98, (2023 Aug 11).

[13] Leve Z, Ross N, Pokpas K, Carleschi E, Doyle BP, Abraham Sanga N, Mokwebo KV, Iwuoha E. Synthesis and characterization of palladium/silver modified reduced graphene oxide–nanocomposite platform for electrochemical sensors. ChemistrySelect. **9**(17), e202400606, (2024 May 3).

[14] Mahan NK, Al Marjani MF, Abd Aziz MS, Johari AR, Talib SQ, Krishnan G. SUPERIOR ANTIBACTERIAL PROPERTIES OF COPPER-BEARING HIGH ENTROPY ALLOY COATED STAINLESS STEEL SURFACE FABRICATED USING LASER CLADDING. Jurnal Teknologi (Sciences & Engineering). **86**(6), 153-63, (2024 Sep 17).

[15] Urabe AA, Aziz WJ. Biosynthesis of cobalt oxide (Co3O4) nanoparticles using plant extract of Camellia sinensis (L.) Kuntze and Apium graveolens L. as the antibacterial application. World News of Natural Sciences. **2019**(24),356-64.

[16] Singh J, Dutta T, Kim KH, Rawat M, Samddar P, Kumar P. ‘Green’synthesis of metals and their oxide nanoparticles: applications for environmental remediation. Journal of nanobiotechnology. **16**(1), 84, (2018 Oct 30).

[17] Hasan S, Khashan KS, Hadi AA. Laser-induced synthesis of palladium@ Silver core–shell nps as an effective antibacterial agent. Plasmonics. **18**(2), 689-99, (2023 Apr).

[18] Mahan NK, Al-Marjani MF, Krishnan G, Salman MA. Characterization and Antibacterial Properties of CoCrCuFeNi High-Entropy Alloy Nanoparticles Synthesized by Lactobacillus acidophilus. Plasmonics. **20**(8), 5857-65, (2025 Aug).

[19] Mahan NK, Hassan MA, Mohammed AH, Khalee RI. Neuronal Toxicity of CdS Nanoparticles Prepared by Laser Ablation and their

Effect on Liver. InMaterials Science Forum, Trans Tech Publications Ltd. **1039**, 537-556 (2021).

[20] Kozlovskiy AL, Kenzhina IE, Zdorovets MV. FeCo–Fe2CoO4/Co3O4 nanocomposites: Phase transformations as a result of thermal annealing and practical application in catalysis. Ceramics International. **46**(8), 10262-9, (2020 Jun 1).

[21] Zdorovets MV, Kozlovskiy AL. Study of phase transformations in Co/CoCo2O4 nanowires. Journal of Alloys and Compounds. **815**, 152450, (2020 Jan 30).

[22] MubarakAli D, Kim H, Venkatesh PS, Kim JW, Lee SY. A systemic review on the synthesis, characterization, and applications of palladium nanoparticles in biomedicine. Applied Biochemistry and Biotechnology. **195**(6), 3699-718, (2023 Jun).

[23] Urabe AA, Nayef UM, Kamel R. Preparation and characterization of Pd nanoparticles via second harmonic Nd: YAG laser ablation and deposited on porous silicon for photo-conversion application. Journal of Optics. **53**(1), 1-9, (2024 Feb).

[24] Salman SH, Khashan KS, Hadi AA. Green synthesis and characterization of palladium nanoparticles by pulsed laser ablation and their antibacterial activity. Metals. **13**(2), 273, (2023 Jan 30).

[25] Ivanisenko Y, Kurmanaeva L, Weissmueller J, Yang K, Markmann J, Rösner H, Scherer T, Fecht HJ. Deformation mechanisms in nanocrystalline palladium at large strains. Acta Materialia. **57**(11), 3391-401, (2009 Jun 1).

[26] Urabe AA, Nayef UM, Kamel R. External magnetic field effect on synthesis palladium nanoparticles via laser ablation deposited on porous silicon as a gas sensor application. Journal of Optics. **53**(4), 2870-6, (2024 Sep).

[27] Ando S, Yamamoto E, Kobayashi M, Osada M. Atomic layer engineering of Pd nanosheets for an enhanced hydrogen evolution reaction. Nano Letters. **24**(36), 11239-45, (2024 Aug 5).

[28] Urabe AA, Nayef UM, Kamel R. Photocatalysis application for palladium nanoparticles synthesized by laser ablation in liquid. Plasmonics. **19**(2), 611-9, (2024 Apr).

[29] Sattar ZA, Mohammed AM, Khalaf YH. Green synthesis of Curcuma longa-mediated Palladium nanoparticles as antioxidant, antimicrobial, and anticancer agents. Results in Chemistry. **9**, 101675, (2024 Jul 1).

[30] Xu L, Wu XC, Zhu JJ. Green preparation and catalytic application of Pd nanoparticles. Nanotechnology. **19**(30), 305603, (2008 Jul 30).

[31] Hasan S, Khashan KS, Hadi AA. Laser-induced synthesis of palladium@ Silver core–shell nps as an effective antibacterial agent. Plasmonics. **18**(2), 689-99, (2023 Apr).

[32] Gao J, Jin Y, Fan Y, Xu D, Meng L, Wang C, Yu Y, Zhang D, Wang F. Fabricating antibacterial CoCrCuFeNi high-entropy alloy via selective laser melting and in-situ alloying. Journal of Materials Science & Technology. **102**, 159-65, (2022 Mar 10).

[33] Jihad MA, Noori FT, Jabir MS, Albukhaty S, AlMalki FA, Alyamani AA. Polyethylene glycol functionalized graphene oxide nanoparticles loaded with nigella sativa extract: a smart antibacterial therapeutic drug delivery system. Molecules. **26**(11), 3067, (2021 May 21).

[34] Mohammad AM, Fatah SK, Majeed MH, Mohammed SM, Mohammed SM. Enhanced antibacterial activity and structural characterization of ZnO-doped MgO nanocomposites synthesized via sol–gel technique. Bionanoscience. **14**(2), 1228-41, (2024 Jun).

[35] Vinodhini S, Vithiya BS, Prasad TA. Green synthesis of palladium nanoparticles using aqueous plant extracts and its biomedical applications. Journal of King Saud University-Science. **34**(4), 102017, (2022 Jun 1).

[36] Mohammad AM, Saleh AM, Ahmed BH, Azeez YH, Fatah SK, Mehranfar H. Comprehensive study on the temperature-dependent properties of Co0. 5Mg0. 5FeCrO4 ferrite nanoparticles: experimental and theoretical analyses. Journal of Sol-Gel Science and Technology. **116**(1), 303-18, (2025 Oct).

[37] Hasan S, Khashan KS, Hadi AA. Antibacterial activity of silver nanoparticles created by one step nanosecond Nd: YAG laser ablation in water. Advances in Natural Sciences: Nanoscience and Nanotechnology. **14**(2), 025013, (2023 Jun 1).

[38] Pathogens CW. Research Journal of Pharmaceutical, Biological and Chemical Sciences Antimicrobial Activity of the Ethanolic Extract of Coleus aromaticus against. **5**, 1286-96.

[39] Marhaba S. Optical response of palladium nanocube singles and dimers: Plasmon coupling effect between nanoparticles. Next Materials. 9, 101108, (2025 Oct 1).

[40] Fatah SK. Synthesis and characterisation of zinc oxide nanopowders prepared by precipitation method.

[41] Ismael GI, Barzani KK. Prevalence and Molecular Characterization of Gram Positive Bacteria Isolated from Autistic Children in Erbil City. Passer Journal of Basic and Applied Sciences. **8**(1), 62-71, (2026 Jul 1).

[42] Issa MA, Ali SH. Molecular Identification and Phylogeny of Endophytic Bacterial Communities Isolated from some Legumes Using 16SrDNA. Passer Journal of Basic and Applied Sciences. **5**(2), 231-6, (2023 May 16).

[43] Ahmed LA, Aljaf OQ. Extraction, isolation, characterization, and antimicrobial study of a compound in the crude of Oak Gall's. Passer Journal of Basic and Applied Sciences. **5**(2), 318-23, (2023 Aug 3).

[44] Hasan HS, Salih AM, Saadi AT. Molecular Detection of Virulence Factors and Antibiotic Resistance among Enterococcus Species Isolates from Kurdistan Region of Iraq. Passer Journal of Basic and Applied Sciences. **6**(2), 324-32, (2024 May 27).